This is a Preprint and has not been peer reviewed.

Geochemical signatures of rare earth elements and yttrium exploited by acid solution mining around an ion-adsorption type deposit: role of source control and potential for recovery

Haiyan Liu[1, 2, *]; Huaming Guo[3, *]; Olivier Pourret[4, *]; Zhen Wang[1, 2]; Maohan Liu[1, 2]; Weimin Zhang[1, 2]; Zebing Li[1, 2]; Bai Gao[1, 2]; Zhanxue Sun[1, 2]; Pierre Laine[4]

[1] *School of Water Resources and Environmental Engineering, East China University of Technology, Nanchang 330013, P. R. China*

[2]*State Key Laboratory of Nuclear Resources and Environment, East China University of Technology, Nanchang 330013, P. R. China*

[3] *School of Water Resources and Environment, China University of Geosciences (Beijing), Beijing 100083, P.R. China*

[4]*UniLaSalle, AGHYLE, Beauvais, France*

*** Corresponding author:** Haiyan Liu, Huaming Guo, Olivier Pourret

418 Guanglan Road, Jingkai District, Nanchang, P. R. China **(H. Liu)**;

29 Xueyuan Road, Haidian District, Beijing, P. R. China **(H. Guo)**

19 rue Pierre Waguet-BP 30313, 60026 Beauvais, France **(O. Pourret)**

E-mail address: hy_liu@ecut.edu.cn (H. Liu); hmguo@cugb.edu.cn (H. Guo); olivier.pourret@unilasalle.fr (O. Pourret)

Abstract: Elevated concentrations of rare earth elements and yttrium (REE+Y) in acid mine drainage (AMD) attract worldwide attention. However, the source and control of REE+Y distribution patterns in AMD remain unclear. Water, rock, sediment, and sludge samples were collected from an ion-adsorption deposit site to investigate REE+Y concentrations and distributions. The heavy REE (HREE)-enriched patterns of the AMD resulted from preferential desorption of HREE in the clay-rich sediment strata, from which the REE+Y were ion-exchanged by an in-situ underground leaching process using ammonium sulfate brine. Free ions and sulfate complexes preserved REE+Y patterns and facilitated REE+Y mobility in the AMD leachate system. High concentrations of REE+Y occurred in the AMD, and decreased progressively through nitrification-denitrification and coagulation-precipitation procedures in a water treatment plant. Concentrations of REE+Y were one to three orders of magnitude higher in AMD than those in groundwater, and were negatively correlated (r^2 = –0.72) with pH (3.8 to 8.7), suggesting that an acid desorption from minerals contributed the REE+Y to the AMD from the source rock. Normalized REE+Y patterns showed enrichments of HREE over light REE (LREE) and negative Ce anomaly. The distribution patterns were relatively constant for all water samples, despite their huge difference in REE+Y concentrations. This suggested a limited impact of preferential precipitation of LREE over HREE on REE+Y fractionations during neutralization. The potentially recoverable LREE and HREE were calculated to range between 1.12 kg/day and 3.37 kg/day, and between 1.29 kg/day and 3.76 kg/day, respectively. The findings reported in this study lends promise for efficient

REE+Y recovery from AMD.

Keywords: Lanthanide; Acid mine drainage; Water-rock interaction; Fractionation; Critical metals

1. Introduction

Global demand of rare earth elements and yttrium (REE+Y) to support technology has increased in the past two decades (Haxel et al., 2002; Van Gosen et al., 2014), leading to increased production of rare-earth oxides (U.S. Geological Survey, 2021). China sustains 98% of global REE+Y demand with an ion-exchange processed clay deposit in southern China as a major supplier for middle REE (MREE) and heavy REE (HREE) (Alonso et al. 2012). The REE+Y were mainly mined via heap leaching, and this technology produced a large amount of acid mine drainage (AMD) and mine tailings (Liu et al., 2019b). The AMD potentially migrating into subsurface environments imposed severe REE+Y contamination to soils, waters, and crops (Liu et al., 2019a; Liu et al., 2020). The thus increased REE+Y emissions to the environment have caused worldwide concerns (Vaziri Hassas et al., 2021; Ayora et al., 2016).

Acid mine drainage is generated through oxidation of sulfides (e.g., pyrite) contained in target strata upon ADM has acidic pH and contains elevated sulfate and metal(loid)s (Nordstrom and Alpers, 1999; Gimeno et al., 2000; Nordstrom et al., 2015). The highly polluted AMD has been considered a severe environmental problem posing great risks to the environment near the exploited mine. This issue is of global concern (e.g., in China, Vietnam, Australia, India and Spain) (Akcil and Koldas, 2006; Marquez et al., 2018, and references therein). AMD could be treated by passive natural attenuation like microbial activity, or by active technology requiring external input of energy and material to maintain in continuous operation (Johnson

and Hallberg, 2005). However, both technologies have drawbacks such as bioclogging and scaling problems resulting from mineral precipitation for the former, and costly and time-consuming processing for the latter (Léon et al., 2021).

Acid mine drainage has also been shown to contain high levels of REE+Y (Verplanck et al., 2004; Moraes and Ladeira, 2021). Owing to their spectroscopic and magnetic properties, the REE+Y have been widely used in clear energy producing, medical diagnosis, and other applications (Wall, 2014; Van Gosen et al., 2014). This has resulted in increased demand of REE+Y for the world's market. Therefore, seeking alternative sources of REE+Y (esp. HREEs: Dy, Tb, Eu and Yb) is an important need for development of recovery technology in many countries (Binnemans et al., 2013).

REE+Y recovery from AMD and its sludges were investigated by a number of studies (Stewart et al., 2017; Vass et al., 2019; Zhang and Honaker, 2020). Previous research at various mine sites showed that the REE+Y concentrations in AMD were several orders of magnitude higher than the median values of near-neutral mine waters (Ayora et al., 2016). The normalized REE+Y patterns were characterized by MREE enrichment over LREE and HREE. Some studies showed LREE- (Bozau et al., 2004) and HREE- (Medas et al., 2013) enriched normalized patterns in AMD as well. Other studies reported that AMD was depleted in LREE (Gammons et al., 2003; Sharifi et al., 2013; Migaszewski et al., 2014).

In spite of the known normalized REE+Y patterns in AMD systems, the underlying mechanism regulating the formation of the patterns is poorly understood.

Considering the extremely low concentrations of REE+Y in rainwater (Zhang and Liu, 2004; Zhu et al., 2016), REE+Y are ultimately sourced from water-rock interactions. Preferential leaching of REE-bearing solids was proposed for causing the enrichment patterns (Sun et al., 2012; Wallrich et al., 2020, and references therein). In this framework, REE+Y-enriched mineral phases should be present in the bulk solid samples. Indeed, sequential extraction of strata rocks showed that the REE content was related to carbonate and aluminosilicate minerals (Worrall and Pearson, 2001). After being removed by ion-exchange, the rock samples were extracted sequentially with acidic solutions buffered at pH 1.6, 3.6, and 5.5, to simulate the formation process of AMD, showing that the sequential extracts had similar REE patterns to those of AMD (Worrall and Pearson, 2001). Results of Worrall and Pearson's (2001) experiments further demonstrated that REE signatures in acidic water were a mixture of leachates of various sedimentary mineral components, suggesting that REE+Y enrichment patterns for AMD were of source-control. Furthermore, the conservative behavior of REE+Y in the acidic solutions had accounted for their long-distance transport (Verplanck et al., 2004). However, other studies indicated that process-derived reactions such as fractionation by colloidal complexes (Åström and Corin, 2003), adsorption-desorption on surface coatings (Åström, 2001), differences in solutes complexation (Dia et al., 2000), and preferential precipitation of certain REE during formation of secondary minerals (Elderfield et al., 1990; Leybourne et al., 2000) were responsible for the deviating REE+Y enrichment patterns. A recent study suggested that the roles of geology in controlling REE+Y distribution and patterns in

AMD might be complicated by geochemical, biological and environmental factors (León et al., 2021). The coherent properties and predictable behavior of REE+Y make them ideal tracers of clastic sediment transport (Taylor and McLennan, 1988), water-rock interactions (Worrall and Pearson, 2001), and mixing processes (Liu et al., 2017a). The unique properties of REE+Y constitute therefore an opportunity to study the source, origin, fate and transport of AMD, which is important in addressing the mechanisms of AMD formation and contamination.

The hypotheses for this study were: (i) high REE+Y concentrations occur in AMD where elevated metal, sulfate and ammonium concentrations co-occur, (ii) local lithology in relation to acidification-enhanced desorption and scavenging by secondary minerals controls REE+Y distribution patterns in AMD, and (iii) the REE+Y inventory of AMD is potentially recoverable upon pH neutralization by implementing appropriate treatment options. The objectives of this study were to: (i) investigate the concentrations and distributions of REE+Y in an AMD system (i.e. water, rock, sediment, and sludge), (ii) characterize the geochemical controls of REE+Y sources and fractionation patterns in AMD, and (iii) assess the potential of REE+Y recovery from AMD.

2. Methods and materials

2.1 Regional hydrogeological settings

The mining site (longitude: 114°47′28″, latitude: 24°54′25″) is located in the Jiangxi province, southern China (Fig. 1), and has a subtropical monsoon climate. The temperature ranges from 39°C to -3.1°C (recorded historically), with an annual

131 average of 19.7 °C. Precipitation ranges from 1058 to 2190 mm (annual average 1608
132 mm), dominating from April to July (accounts for 60%). Annual evaporation is 1497
133 mm (1349 to 1619 mm), intensely occurring in July and August. The drainage basin
134 has five main rivers that are connected to the tributaries of Dongjiang River running
135 from south to north with an annual average flow rate of 14 m^3/s.

136 Late Cretaceous to Quaternary strata outcrop in the mine area, of which
137 Cambrian, Devonian and Jurassic strata are exposed in most areas and are distributed
138 primarily in the eastern and southern part of the study area. The mine is hosted in
139 Jurassic to early-Cretaceous igneous rocks, which cover a total area of 360 km^2. The
140 main rocks are micaceous granite, porphyry granite, monzonitic granite, and diorite
141 (Yang et al., 2013). The REE+Y are concentrated in two types of micaceous granite,
142 namely muscovitic granite and biotitic granite, where HREE and LREE have distinct
143 distribution patterns in their weathered layers (Yang et al., 2013). The HREE
144 accounted for 75 to 89 wt.-%, with an average value of HREE/LREE of 4.4 in the
145 weathering regoliths of muscovitic granite. The average HREE proportion was 61%,
146 and the HREE/LREE value was 1.6 for the biotitic granite counterpart. The thickness
147 of the strongly-weathered regolith layer ranges from 5 to 25 m with a corresponding
148 mineral inventory of mainly quartz, feldspar and mica.

149 Groundwater in the mine area is mainly hosted in the fissure network of
150 medium-grain micaceous granite and largely belongs to the phreatic water type. The
151 hydrochemical facies include Ca-SO_4, Ca-SO_4-HCO_3, Ca-Cl, and Ca-HCO_3-Cl type
152 waters with total dissolved solids (TDS) ranging from 17 to 170 mg/L.

Heap and pond leaching was used previously as an active mining technology at this mine site. However, it has been banned by Chinese government due to great vegetation damage. In-situ leaching is currently done by injecting acidic ammonium sulfate solution through wells drilled into the sedimentary ore deposit. The acidic leachate solution containing the dissolved metals pumped out poses environmental risks as well. Ammonium has been reported to exceed the threshold recorded in groundwater quality standard (Liu et al., 2019b). The main REE leaching mechanism as shown by Eq. (1) is an ion-exchange reaction with ammonium (NH_4^+) from clay minerals in the sedimentary deposit (Chi and Liu, 2019):

$$(Al_4Si_4O_{10}(OH)_8)_m \cdot nREE^{3+} + 3nNH^{4+} = (Al_4Si_4O_{10}(OH)_8)_m \cdot (NH^{4+})_{3n} + nRE^{3+} \quad (1)$$

Although not AMD in sensu-stricto, the acidic mine waters recovered from this solution mining process are termed AMD as well in the following. A sewage treatment plant (STP) was established at the mine site to process the acid efflux from the mine. The STP technology mainly consists of three procedures, which are (i) nitrification-denitrification to remove ammonium, (ii) coagulation-precipitation to remove metals, and (iii) dilution of treated water with original mine water. Finally, the mixture is discharged into rivers down-stream.

2.2 Sample collection

Sixteen water samples were collected in July 2020. Among them, five were AMD samples (MW1 to 5), six were effluents of STP undergoing nitrification-denitrification treatment procedures (NDT1 to 6), four were effluents going through coagulation-precipitation treatment processes (CPT1 to 4), and one was

water sample collected from a local groundwater (GW) well in a village near the mine. All water samples were filtered with 0.22 μm pore size cellulose acetate membranes. Samples for cation and trace element analysis were stored in 50 mL high-density polyethylene (HDPE) bottles and were acidified to pH <2 with HNO_3. Samples for anion analysis were stored in HDPE bottles without acidification. Samples for DOC analysis were sampled in 30 mL amber glass bottles and acidified to pH <2.0 by admixing 1:9 (v/v) H_2SO_4. Samples for REE+Y analysis were sampled in 500 mL HDPE bottles following an acidification with HNO_3. Sampling locations are shown in Fig. 1.

Two rock samples (R1 and R2) were sampled from the outcrop. Three surface sediment samples (MW1-SS, MW2-SS and MW3-SS) were collected from the locations where mine water samples (MW1, 2, and 3) were taken (Fig. 1). The surface sediment samples were collected down to a depth of about 30 cm below land surface. Sludge samples (MW4-SG, MW5-SG and CPT1-SG) were taken from the bottom precipitates of the settling pond and creek bed, while NDT2-SG and NDT3-SG were sludge samples collected by using a vacuum hose that was deployed to the bottom of a huge container having a depth of about 6 m. All the rock, sediment and sludge samples were stored in clean plastic bags.

2.3 Analytical methods

Physicochemical parameters of the water samples, including temperature, pH, electrical conductivity (EC), and redox potential, were measured with a HI 9828 portable multi-meter (HANNA, Woonsocket, RI, USA). To minimize the influence of

atmospheric contact, the monitoring probe was immersed in an in-line flow cell where water was pumped through constantly. Physiochemical data were recorded in the field once stabilized. Alkalinity was titrated immediately in the field by using a Model 16900 digital titrator (HACH, Loveland, USA). Redox sensitive components such as total Fe, Fe(II), NH_3-N, NO_2-N, and S^{2-} were quantified using a portable UV/VIS spectrophotometer (HACH, DR2800). This device was calibrated with holmium oxide filter and holmium oxide wavelength standard solution.

Anions were analyzed by a lab-based ion chromatography system (ICS2000, Dionex, Thermo Fisher Scientific, Waltham, USA). Cations and trace elements were determined by using inductively coupled plasma optical emission spectrometry (ICP-OES iCAP6300, Thermo Fisher Scientific, Waltham, USA) and inductively coupled plasma mass spectrometry (ICP-MS 7500C, Agilent Technologies, Santa Clara, USA), respectively. Six standard solutions, diluted from stock standards (AR, Tanmo Quality Inspection Technology, China), were used to calibrate the instrument. Only the standard curves with correlation coefficient (r^2) better than 0.9999 were used for subsequent analysis. The results were verified with replicate samples to ensure an analytical precision better than 5%.

Analysis of REE+Y concentrations were performed by employing two different single-collector inductively coupled plasma sector field mass spectrometry instruments (ICP-SFMS ELEMENT XR and ELEMENT 2, Thermo Fisher Scientific, Bremen, Germany) based on the protocol published by Rodushkin et al. (2018). A cation exchange resin (AG 50W-X8, 200 to 400 dry mesh size, Bio-Rad laboratory

AB, Solna, Sweden) was used for the preconcentration of REE+Y. Prior to use, the resins were immersed in 14 mol/L HNO_3 overnight and were cleaned with deionized water. A 2 mL low-density polyethylene (LDPE) column was loaded with the prepared resins, and 4 mL 14 mol/L HNO_3 (AR, Sinopharm, China), 8 mL deionized water and 4 mL 9.5 mol/L HCl (AR, Sinopharm, China) were loaded sequentially for conditioning. Finally, a 200 mL sample was introduced into the pre-conditioned column and the retained REE+Y were eluted with 4 mL 0.5 mol/L HCl. By this method, a 50-fold preconcentration was achieved. The REE+Y recovery ranged between 90% and 103%. Calibration and quality control samples were prepared in 2% nitric acid with a stock solution. A medium resolution mode (MR, m/Δm approximately 5400) was set up for monitoring the isotopes ^{146}Nd, ^{147}Sm, ^{151}Eu, ^{163}Dy, ^{165}Ho, and ^{172}Yb, and a high resolution mode (HR, m/Δm approximately 12000) was used for monitoring the isotopes ^{139}La, ^{140}Ce, ^{141}Pr, ^{157}Gd, ^{159}Tb, ^{166}Er, ^{169}Tm, and ^{175}Lu, as suggested by Wilkin et al. (2021). The detection limits were 0.1 ng/L for Lu, 0.2 ng/L for Eu, and 0.5 ng/L for other REE and Y. One ng/L In solution was used as internal standard to check for the mass bias. Interferences of BaO^+ on the ^{151}Eu and ^{153}Eu isotopes were corrected automatically by setting up a correction measure during analysis. Briefly, we run ~100 μg/L Ba and determine the peak area of the Eu isotope being monitored. During a run of samples, Ba (without calibration) was monitored and the results were applied for a correction. The analytical precision of replicate samples of REE+Y were generally better than 8%.

Bulk composition analysis of sediment and sludge samples were carried out

using a $LiBO_2$-LiB_4O_7 fusion and X-ray fluorescence (XRF ARL Advant X), and after dissolving the glass disks by dilute nitric acid also by ICP-OES and ICP-MS. Mineral compositions in sediment and sludge were determined by X-ray diffraction (XRD D8 advance, Bruker) with a CuKα radiation. Diffraction patterns were scanned at 2θ of 20° to 70° and a step size of 0.02°. Minerals having content greater than 5 wt.-% of the bulk solid were thus identified.

Solid samples and suspended matter filtered out of aqueous solutions were examined additionally by using scanning electron microscopy (SEM) (NovaNanao 450, Fei Czech, Co., Ltd.).

2.4 Modelling approach

Speciation calculations were performed using the hydrogeochemical code PHREEQC version 3.4 (Parkhurst and Appelo, 2013) with the Nagra/PSI database (Hummel et al., 2002). Stability constants of REE complexation to major anions (e.g. CO_3^{2-}, SO_4^{2-}, OH^-, Cl^-, F^-, and NO_3^-) were incorporated into the database from literature (Table S1) (Supporting Information). For example, constants for $REE(CO_3)_2^-$ and $REECO_3^+$ were taken from Luo and Byrne (2004), and those for $REESO_4^+$ were taken from Schijf and Byrne (2004). Surface complexations of REE onto iron oxyhydroxides were considered as previously done by Liu et al. (2017b), in which the relevant formation constants and detailed modelling procedures were provided. Statistical tests were performed using Grapher (version 10.0) and IBM SPSS Statistics (version 19.0) programs.

3. Results

263 3.1 Water chemistry

264 Major ion concentrations and physicochemical parameters are compiled in Table
265 S2. Results revealed that mine waters (MW1 to 5) had pH values between 3.8 and 4.2.
266 A slight increase in pH (4.1 to 4.9) was observed for NDT samples (NDT1 to 6). The
267 CPT samples had pH values > 7 (7.4 to 8.7), and the GW sample's pH was 6.5.
268 Generally, pH values increased from the regions nearest to the mine site to
269 downstream of the STP facility.

270 All water compositions are shown on a Piper plot for comparison (Fig. 2). The
271 TDS ranged between 95 and 562 mg/L (average 363 mg/L) with the lowest values in
272 GW. Before passing through the STP (i.e., samples MW 1 to 5), cation compositions
273 were predominated by Ca^{2+} and Mg^{2+}, and NO_3^- and SO_4^{2-} were the dominant anions,
274 while Cl^- concentrations were < 5 mg/L. Water types thus determined for MW 1 to 5
275 were Ca/Mg-SO_4 and Ca/Mg-HCO_3/SO_4. Over the CPT pathway (CPT 1 to 4), the
276 major cation composition shifted towards Na^+ predominance (52 to 104 mg/L),
277 followed by Mg^{2+} (23 to 26 mg/L) and Ca^{2+} (31 to 48 mg/L), while the dominant
278 anion was HCO_3^- (>156 mg/L), hydrochemical type for these samples being
279 Na-Ca/Mg-HCO_3. This type of water continued downstream near the village (CPT 4),
280 approximately 1 km downstream from the STP. The NDT samples showed a coherent
281 water type of Mg-Na-Ca-HCO_3-SO_4. The GW collected from the village was of
282 Na-HCO_3 water type.

283 Total dissolved Fe (Fe_T) concentration ranged from 0.23 to 0.48 mg/L (average
284 0.31 mg/L) in MW samples, while it dramatically decreased to a range of 0.05 to 0.20

mg/L (average 0.08 mg/L) after passing through the NDT procedure. A further decease in Fe_T concentration occurred in water which went through the CPT (0.03 to 0.07 mg/L, average 0.06 mg/L). The lowest Fe_T concentration was observed in GW (0.006 mg/L, i.e. near detection limit). Ferrous presumably dominated the Fe species in MW and NDT water samples due to the high Fe_T concentrations. For CPT and GW samples, Fe(II) concentrations were below detection limits, with an exception of CPT 4 which had a Fe_T concentration of 0.02 mg/L (Fig. 3a).

Total dissolved Al (Al_T) concentration ranged between 3.04 and 5.64 mg/L (average 4.7 mg/L), and between 1.77 and 2.57 mg/L in MW and NDT samples, respectively. Concentrations of Al_T decreased to < 0.3 mg/L in CPT samples. No Al_T could be detected in GW. Total dissolved Mn concentrations were generally higher in MW samples (2.00 to 5.36 mg/L, average 3.09 mg/L), as compared to those in NDT (2.14 to 2.61 mg/L, average 2.45 mg/L) and CPT (1.14 to 2.12 mg/L, average 1.63 mg/L) samples. Other trace element concentrations, including Pb, Zn, Sr, Rb, and U, all decreased substantially after the CPT procedure (Fig. 3b).

3.2 Aqueous REE+Y distribution patterns

Total concentrations of REE+Y (ΣREE+Y) in water samples are presented in Table S3. The ΣREE+Y concentrations ranged from 3.84 to 4.33 mg/L (average 4.11 mg/L), and from 1.67 to 2.97 mg/L (average 2.21 mg/L) in MW and DNT samples, respectively. These values were up to two orders of magnitude higher than the ΣREE+Y concentrations of CPT samples (0.07 to 0.19 mg/L, average 0.12 mg/L), and were more than three orders of magnitude higher than the ΣREE+Y concentrations in

GW sample (5.3 μg/L, Fig. 3a).

Upper continental crust normalized REE+Y patterns were characterized by HREE enrichment over LREE and negative Ce ($Ce/Ce^* = Ce_{UCC}/(La_{UCC} \times Pr_{UCC})^{0.5}$) (Fig. 4). The average normalized $(Yb/Nd)_{UCC}$ ratio (as a fractionation measure) was higher in CPT samples (10.23) as compared to MW (7.11), NDT (7.76), and GW (5.70) samples. The Ce anomaly was < 0.3 with an exception of GW ($Ce/Ce^* = 0.37$) (Table S3). Positive Y anomaly ($(Y/Ho)_{UCC}$) was observed in MW (1.14 to 1.53, average 1.29) and NDT (1.21 to 1.36, average 1.33) samples. Value of $(Y/Ho)_{UCC}$ was > 1.70 for CPT samples, and was 1.39 for the GW sample.

3.3 Modelling results

Free (REE^{3+}) and sulfate ($REESO_4^+$) complexes dominated lanthanide species in MW and NDT samples (Figs. 4b and d). The LREE tended more to be associated with SO_4^{2-}, while the HREE were dominantly present as free ions. The average proportion of La occurring as $REESO_4^+$ was 48%, and 36% for Lu. Carbonate ($REECO_3^+$ and $REE(CO_3)_2^-$) and nitrate complexes ($REENO_3^+$) were < 5% in proportion of all lanthanide species. The lanthanides in CPT samples were calculated mainly in carbonate complex forms of $REECO_3^+$ and $REE(CO_3)_2^-$ that accounted for 73% to 98% for La and 89% to 99% for Lu. Free ions made up 6% for La and < 1% for Lu (Fig. 4f). Lanthanides in the GW sample were predicted to occur as free ions, $REECO_3^+$ + $REE(CO_3)_2^-$, and $REESO_4^+$. The proportions of these three species were predicted to be 49% to 79%, 5% to 34%, and 7% to 15%, respectively (Fig. 4h). $REENO_3^+$ mostly accounted for < 2% of total lanthanide speciation. The other

potential species, including hydroxyl and chloride complexes, were < 1% in the water samples.

3.4 Geochemical and mineralogical properties of solids

The rock samples were dominated by SiO_2 (66 to 68 wt.-%), while Al_2O_3 was the second most abundant component (9 to 18 wt.-%), followed by Fe_2O_3 (4 to 7 wt. %) (Table S4). Composition of surface sediment samples ranged from 61 to 76 wt. % for SiO_2, 10 to 3 wt. % for Al_2O_3, and 2 to 5 wt. % for Fe_2O_3. Other metal oxides were generally < 6 wt. %. For the sludge samples, SiO_2 contents ranged from 60 to 67 wt. %, Al_2O_3 from 15 to 18 wt. %, and Fe_2O_3 from 3 to 12 wt. %. Other metal oxides were < 5 wt.%.

Contents of ΣREE+Y in sludge samples ranged between 0.80 mg/kg and 44.74 g/kg (average 19.95 g/kg). Those values were much higher than the ΣREE+Y contents of rock (0.33 to 0.85 g/kg, average 0.66 g/kg) and sediment samples (0.35 to 0.43 g/kg, average 0.39 g/kg) (Table S5). UCC-normalized REE+Y patterns showed that all samples were enriched in HREE relative to LREE and had negative Ce anomaly. The $(Yb/Nd)_{UCC}$ values ranged from 6.14 to 9.14, from 3.51 to 5.83, and from 1.08 to 2.10 in sludge, sediment and rock samples, respectively (Table S5). Normalized REE+Y patterns of sludge and sediment samples showed an increasing upward trend from La to Sm, and a relatively flat trend from Tb to Lu (Fig. 5). On the other hand, REE+Y patterns for rock samples showed a slightly increasing trend with atomic numbers, indicating that a higher degree of HREE enrichment over LREE occurred for sludge and sediment samples as compared to rock samples. The Ce anomaly

ranged from 0.18 to 0.63, and from 0.61 to 0.79, in sludge and sediment samples, respectively. Rock samples showed weakly negative Ce anomalies (Ce/Ce* ~0.98) (Table S5).

SEM imaging of filter residuals showed that the mine waters contained many suspended aggregate particles with diameters larger than 0.22 μm. This was more commonly observed in CPT samples as compared to MW samples (Fig. S1). Sediment samples contained clastic textures on the surfaces with length <1 μm (Fig. S2). On the surfaces of sludge samples, needle-like and burr-like shapes occurred with shorter length than those observed in sediment samples (Fig. S2).

Results of XRD show that quartz (56% to 68%), muscovite (7% to 11%), kaolinite (8% to 14%), feldspar (both albite ($NaAlSi_3O_8$) and microcline ($KAlSi_3O_8$), 10% to 14%), schwertmannite (< 5%), and ferrihydrite (< 5%) were present in the sediment samples (Fig. S3). For sludge samples, quartz was determined to account for 27% to 47%, feldspar 10% to 27%, and schwertmannite 15% to 24%. Other minerals mostly showed contents < 5%.

4. Discussion

4.1 Geochemical characteristics

The average values of REE concentrations in the acid mine waters were several orders of magnitude higher than those in natural near-neutral waters (Ayora et al., 2016). Specifically, the average total REE (ΣREE) concentrations in our samples (0.003 to 2.18 mg/L, average 0.94 mg/L) were comparable to the values reported by Liu et al. (2019a) (up to 10.86 mg/L, average 1.14 mg/L) found for the same study

area. The MW samples showed higher ΣREE+Y concentrations than NDT, CPT and GW samples. With MW water moving downstream the processing line, ΣREE+Y concentrations decreased (Fig. 3a). Trends of Fe, Al, and Mn concentrations were similar to those of ΣREE+Y concentrations (Fig. 3a), indicating that REE+Y exhibited similar behavior to these metals. Indeed, the Fe, Al and Mn concentrations were positively correlated with ΣREE+Y concentrations, with correlation coefficients (r^2) of 0.61 ($p < 0.01$), 0.86 ($p < 0.01$), and 0.43 ($p < 0.01$) (Fig. 6a), respectively, indicating that REE+Y behaved more like Al than Mn or Fe. The positive correlation indicated intense leaching of these cations and a close association of REE+Y with Fe, Mn and Al in particulate phases (Zhou et al., 2012).

Samples with higher ΣREE+Y concentrations also contained relatively higher SO_4^{2-} and NO_3^- concentrations (Table S2 and S3). Although a poor positive correlation was observed between SO_4^{2-} and ΣREE+Y concentrations ($r^2 = 0.18$, $p = 0.1$) (Fig. 6a), the predominance of SO_4^{2-} in total anions could be observed in MW samples (Fig. 2). This was largely due to the use of ammonium sulfate as an in-situ extractant for REE+Y mining (Liu et al., 2019b). Similarly, anthropogenic pumping of ammonium sulfate would account for the high NO_3^- concentrations, and the relatively constant NO_3^- concentrations in CPT samples demonstrated that nitrification reactions occurred under these conditions. It should be noted that, in addition to Fe, Al, Mn, SO_4^{2-} and NO_3, high concentrations of NH_3-N (mostly >10 mg/L) were found to co-occur with REE+Y in AMD. The ΣREE+Y occurrence was therefore attributed to geochemical characteristics of source deposit as well as anthropogenic alterations.

395 4.2 Origin and mobility of REE+Y

396 Previous investigations of AMD suggested that REE+Y originated from leaching
397 of acid soils (Åström, 2001). Other studies attributed REE+Y source to dissolution of
398 REE+Y-bearing minerals in host rocks (Pérez-López et al., 2010; Cánovas et al., 2020;
399 Wallrich et al., 2020). The UCC-normalized REE+Y pattern similarity between acid
400 leachate water and sediment indicates that REE+Y in AMD were derived from
401 sediments directly (Fig. 5). The HREE enrichment in the rock samples suggested that
402 the parent rock acted as the original REE+Y source for the clay-rich sediment layers
403 leached by the acidic waters. Therefore, origin of REE+Y in the AMD highly
404 depended on the REE+Y-bearing mineral phases in the bedrocks, and weathering of
405 bedrocks and desorption from the weathering product minerals were a main pathway
406 mobilizing REE+Y into mine water. The REE+Y would be initially mobilized
407 naturally, when rainwater infiltrated underground (Nesbitt, 1979). The acidic water in
408 contact with the host rock led to a preferential dissolution of weathered minerals like
409 feldspars (Nordstrom et al., 2015). Upon REE+Y being mobilized from the rocks, the
410 majority of them were scavenged via ion exchange by clay-rich sediments/soils. A
411 zone of soils/sediments was formed after weathering of rock crust in the study area,
412 where igneous rocks, mainly composed of acidic granites, were exposed in a large
413 area (Yang et al., 2013; Chi and Liu, 2019). The ion-exchanged REE+Y were readily
414 desorbed from the sediments by acid leaching, where the acid extractant (ammonium
415 sulfate) was injected into the soil/sediment layer. The coherent HREE-enriched
416 patterns in all water samples indicated that the desorbed REE+Y were ultimately

discharged into streams/creeks, and were transported in form of sulfate complexes and free ions until solution conditions became neutral or weakly alkaline as discussed below. Consequently, REE+Y compositions were originally derived from the parent rocks and were immobilized by sediments via sorption, and ion exchange might mobilize REE+Y into the aquifer and surface waters.

4.3 Control on REE+Y concentrations

Concentrations of REE+Y in the investigated acidic waters were controlled by the bulk solution chemistry and co-precipitation of secondary minerals. A negative correlation (r^2 = -0.72, $p < 0.01$) was observed between pH values and ΣREE+Y concentrations. The lowest pH occurring in MW favored leaching of REE+Y-containing minerals in sediment (Dia et al., 2000; Worrall and Pearson, 2001; Janssen and Verweij, 2003). This controlled REE+Y concentrations in the source areas, as reflected by high ΣREE+Y concentrations in MW and NDT samples where pH < 4.9 occurred (Fig. 3a). A decrease in ΣREE+Y concentrations in CPT samples was due to REE+Y scavenging via ion-exchange and/or adsorption by secondary minerals resulting from increased pH values (> 7.4). Similar decreasing trends of Fe, Mn, Al, and SO_4^{2-} concentrations with MW water moving CPT indicated that Fe-, Mn- and Al-bearing minerals were possible secondary phases to scavenge REE+Y in CPT samples (Fig. 3a). Results of XRD supported that clay minerals (i.e. kaolinite), iron oxide (i.e. ferrihydrite), and schwertmannite were the potentially scavenging secondary minerals (Fig. S3). The dominant Fe species shifted from Fe(II) in MW and NDT samples to Fe(III) in CPT (Fig. 3a), suggesting that the formation of ferrihydrite

439 and schwertmannite might occur following Eqs. (2) and (3):

$$4Fe^{2+} + O_2 + 10H_2O = 4Fe(OH)_3(s) + 8H^+ \quad (2)$$

$$8FeSO_4 + 2O_2 + (4 + m)H_2O = Fe_8O_8(OH)_mSO_n + (8\text{-}n)SO_4^{2-} + 2(8\text{-}n)H^+ \quad (3)$$

440 These minerals have been suggested to be most commonly precipitated from AMD
441 during neutralization processes (Lozano et al., 2020a).

442 The positive Y/Ho anomaly was a good indicator for the impact of sorption by
443 solids on ΣREE+Y concentrations (Tweed et al., 2006), as Y behaves differently from
444 Ho during sorption, with Ho having greater affinities than Y for surface complex
445 formation (Bau, 1999), and thus leads to fractionation between them (Nozaki et al.,
446 1997; Möller et al., 1998). The prevailing positive Y/Ho anomaly observed in water
447 samples implied that sorption of REE+Y readily occurred during the neutralization
448 processes (Table S3). Higher Y/Ho values found in CPT samples (1.70 to 1.81) as
449 compared to MW (1.14 to 1.53) and NDT (1.21 to 1.36) samples was attributed to
450 intensive sorption or/and co-precipitation of REE+Y in CPT samples. Indeed,
451 ΣREE+Y concentrations were negatively correlated with Y/Ho values ($r^2 = 0.66$, $p <$
452 0.05), showing that low-pH conditions disfavored REE+Y sorption (De Carlo et al.,
453 1998; Liu et al., 2017b). Scavenging of REE+Y by schwertmannite (Lozano et al.,
454 2020a, b) and Al oxyhydroxides (Ogawa et al., 2019) was recently investigated with
455 different pH ranges. Additionally, changes of REE+Y concentrations might also be
456 coupled to scavenging by Mn oxyhydroxides, with a sorption edge low to pH 4 and a
457 complete REE+Y sorption at pH around 8 (Pourret and Davranche, 2013). However,

458 Mn oxyhydroxides were not detected by XRD in the sludge samples of this study.
459 Therefore, REE+Y concentrations were mainly determined by acidification-enhanced
460 dissolution/desorption/ion exchange from the sedimentary mine body by the acidic
461 ammonium sulfate solution injected, and scavenging by secondary mineral
462 precipitates upon neutralization treatment.

463 4.4 Control on REE+Y patterns

464 All water samples showed enrichments in HREE over LREE when normalized to
465 UCC (Figs. 4a, c, e and g). This pattern has been reported also for AMD and
466 AMD-impacted waters in solution mining for in-situ ion-exchange extraction of
467 REE+Y (Luo et al., 2016). As shown in Fig. 6b, REE+Y patterns of this study and
468 other deposits (Hao et al., 2016; Luo et al., 2016) exploited by the acidic
469 ion-exchange process in southern China were characterized by $(La/Sm)_{UCC}$ and
470 $(Gd/Yb)_{UCC}$. Results showed that all investigated samples were in the quadrant with
471 $(La/Sm)_{UCC} < 1$ and $(Gd/Yb)_{UCC} < 1$, suggesting HREE-enriched patterns (Fig. 6b).
472 These distribution patterns were thought to be mainly controlled by source sediment
473 in this study. The possible mechanisms were addressed as follow.

474 The relatively flat UCC-normalized REE+Y pattern of rocks suggested that the
475 host rock was not a direct cause for HREE enrichment in the acid mine waters. The
476 clear resemblance between REE+Y patterns in sediment and those in the acid mine
477 water indicated that the aqueous REE+Y patterns were probably controlled by the
478 characteristics of the REE+Y sources. The pattern remained relatively constant
479 irrespective of precipitation of secondary minerals with water processing. A model

could be developed as to the formation of HREE enrichment pattern in the acid mine waters, which was that (i) thick zones of clay rich sediment/soil developed above the granites via weathering; (ii) the REE+Y originally mobilized by weathering were sorbed by the sediment layers, whereby a preferential accumulation of HREE by the sediments led to HREE enrichment (Aström, 2001); and (iii) the desorption of previously sorbed REE+Y into the mining solutions, giving rise to enrichments of HREE relative to LREEs in the acidic mine waters (Leybourne et al., 2000; Migaszewski et al., 2016). The desorption process was not expected to significantly fractionate REE+Y in the acid mine waters. This was because: (i) sulfate complex and free ion were the main solution species as indicated by speciation calculations (Fig. 5b), whereby the association of REE+Y with sulfate would not modify REE+Y patterns in aqueous solutions owing to the relatively constant REE+Y-sulfate formation constants (Wilkin et al., 2021); and (ii) REE+Y re-adsorption onto mineral phases was quite limited. This was due to the generally low pH values (<4) in the MW samples, where REE+Y behaved conservatively in spite of Fe and/or Mn oxyhydroxides present (Verplanck et al., 2004; Pourret and Davranche, 2013).

The impact of Fe and Al oxyhydroxide scavenging on HREE enrichment might only be found for the CPT. The low pH values in MW and NDT samples (<4; except for NDT1) disfavor formation of Fe and Al oxyhydroxides (Ogawa et al., 2019). This was why coefficients of distribution of the REE+Y between Al/Fe oxyhydroxide solids and water showed a very weak increase across lanthanide series at pH of 6.3 to 6.8 (Lozano et al., 2020a). This suggested also that HREE fractionation during

enrichment by adsorption or/and co-precipitation with Fe/Al oxyhydroxides was insignificant for this study.

Influence of solution complexation on HREE enrichment in CPT and GW samples was insufficient to significantly fractionate REE+Y in the MW and NDT samples. The most plausible ligand responsible for enrichment of HREE in CPT and GW samples would be CO_3^{2-}, due to preferential stabilization of HREE relative to LREE during REE+Y-CO_3^{2-} complexation (Guo et al., 2010; Liu et al., 2016). Although SO_4^{2-} complexes and free ions were the dominating lanthanide species in MW and NDT samples (Fig. 4), SO_4^{2-} was an almost equally strong complexant for all REE+Y (Wood, 1990). The possibility of HREE enrichment caused by other ligands including OH^-, NO_3^-, PO_4^{3--}, F^- and Cl^- could be excluded either by their low speciation predicted by the model (Fig. 4) or by the preferential complexation of LREE.

Effect of organic matter on HREE enrichment in waters could be ruled out due to preferential complexation of MREE relative to LREE and HREE (Wood, 1993; Pourret et al., 2007) and the low DOC concentrations (generally < 3.2 mg/L). The REE+Y were mostly truly dissolved in the acidic mine waters, and the particulates were less important to control the REE+Y fractionation patterns under pH<4 conditions (Olías et al., 2018).

4.5 Cerium anomaly

A narrow range in Ce anomaly values (Ce/Ce*: 0.21 to 0.29) was observed for all water samples (Fig. 6d). The negative Ce anomaly was controlled by sedimentary

524 REE+Y patterns, where negative Ce anomaly was evident (0.61 to 0.79). Oxidation of
525 soluble Ce(III) to insoluble Ce(IV) that is precipitated as CeO_2 and/or $Ce(OH)_4$ has
526 been recognized as a mechanism immobilizing Ce and resulting in negative Ce
527 anomaly in aqueous solution. This process might have occurred when REE+Y either
528 were initially weathered from host rock or were secondarily mobilized from
529 sediments. The lower Ce/Ce* values in sediments than rocks supported the former to
530 be a more plausible cause for negative Ce anomaly in the acid mine waters. It was
531 unlikely that redox processes played a dominant role in the development of negative
532 Ce anomalies over acid mine water flow, since Ce anomaly was relatively constant in
533 all acid mine water samples despite variable redox conditions. Indeed, Eh-pH diagram
534 regarding the Ce-H_2O system showed that MW and NDT samples mostly were
535 located in stability field of Ce(III), while CPT and GW sample in the stability field of
536 CeO_2 (Fig. 6c). This indicated that Ce initially occurred as free cation when mobilized
537 from sediments, and it tended to be precipitated in form of CeO_2 as pH increased and
538 Eh decreased. In this respect, oxidative scavenging of Ce by Fe oxyhydroxides and/or
539 Mn oxides due to co-precipitation of these secondary minerals might occur in CPT
540 samples (Ohta and Kawabe, 2001; Takahashi et al., 2007). However, this process
541 could not be a dominant control on negative Ce anomaly formation, because the
542 Ce/Ce* values in CPT samples were comparable to those of MW and NDT samples
543 (Table S3), despite that Fe and Mn concentrations decreased substantially with acid
544 mine waters downstream the processing line (Fig. 4a). Therefore, the negative Ce
545 anomaly was suggested to be largely controlled by REE+Y sources in the sedimentary

strata. A similar case was reported by Smedley (1991), showing that Ce anomaly in slightly acidic groundwaters (pH 5.0 - 6.8) was related to rock aquifer as source.

4.6 Implication for REE+Y recovery from AMD

Although AMD has been considered as an environmental concern globally due to its great hazard to ecosystems, it is a potential secondary source of REE+Y as well as coexisting metal elements, which are of economic interest, if appropriate control and treatment processes are implemented. Neutralization of mine water acidity constitutes a simple but promising option for recovering REE+Y from the acid waters. As shown in this study, REE+Y were efficiently sequestrated in CPT samples, where pH values were increased to > 7.4. Correspondingly, high levels of REE+Y were found in precipitate sludge samples, and their concentrations on the g/kg levels were higher than those of source sediments. The yield of REE+Y that were potentially recoverable from acid mine waters were calculated by the difference between loads of REE+Y in original acid mine waters and effluents of the treated mine waters. The loads of REE+Y were obtained by multiplying plant treatment capacity by the REE+Y concentrations in studied waters. Results showed that the recoverable ∑LREE and ∑HREE ranged between 1.11 and 3.37 kg/day, and between 1.29 and 3.76 kg/day, contributing nearly equally between 34% and 38%, and between 38% and 42% of the total ∑REE+Y, respectively. The recoverable Y ranged between 0.79 and 2.35 kg/day (20% to 28%) (Fig. S4). The highest total recoverable value occurred at the location of MW5, which was nearest the inlet of the WTP (Fig. 1).

It must be noted that the profitability of REE+Y recovery from AMD depends on

568 the amounts in AMD, the cost of separation and extraction, and the proportion of
569 HREE over LREE in the AMD (Léon et al., 2021). The high proportions of HREE
570 found in AMD of this area renders recovery of REE+Y from the acid mine waters
571 attractive, considering that HREE are more precious compared to LREE, and that they
572 are largely restricted to South China. The availability of recovering REE+Y as well as
573 other critical metals like Cu, Zn, and Ni from acid mine leachate and their
574 neutralization precipitates were documented by Zhang and Honaker (2020). Ayora et
575 al. (2016) studied the recovery of REE+Y from passive remediation systems of AMD
576 system with two mineral substrate -(schwertmannite and basaluminite) based
577 treatments, showing that AMD remediation process serves as a suitable REE+Y
578 source. Biochar may server as a potential sorbent as well to immobilize these metals
579 in aqueous solution where pH value is acidic (Pourret and Houben, 2018). To sum up,
580 the practical examples of REE+Y recovery from AMD render an environmental
581 problem worthwhile as a source of raw materials, considering that alternative sources
582 of REE+Y is warranted due to an ever increasing demand for these critical metals,
583 particularly for the countries without primary deposits.

584 **5. Conclusions**

585 This study investigated the geochemistry of rare earth element (REE) and
586 yttrium (REE+Y) in acid mine drainage from solution mining. Elevated
587 concentrations of REE+Y were observed in the mine water with low pH. A
588 progressive decrease in REE+Y concentrations occurred with MW flowing through
589 nitrification-denitrification (NDT) and coagulating-precipitation treatment procedures

(CPT). Negative correlation between REE+Y concentrations and pH values ($r^2 = 0.72$) indicated that REE+Y were primarily derived from an enhanced acidic desorption and ion exchange from minerals in the source area. The similarity of HREE-enriched patterns exhibited by AMD to those of source sediment indicated a major role of sediments in controlling REE+Y signatures of AMD. A preferential precipitation of LREE over HREE during the plant treatment process provided for a limited contribution to HREE enrichment in AMD, because the degree of HREE enrichment changed slightly and Ce remained relatively constant in MW, NDT, and CPT samples. Results of XRD and SEM examination indicate that clay minerals (i.e. kaolinite), iron oxides (i.e. ferrihydrite), muscovite, and secondary schwertmannite minerals were the main hosts of REE+Y. Therefore, HREE-enrichment patterns in AMD resulted from preferential desorption of HREE from sediment under the conditions of the in-situ leaching process at the mine site. Free ions and sulfate complexes, which dominated REE+Y species in MW and NTD samples, facilitated the transport of REE+Y and preserved REE+Y patterns during AMD flow. Carbonate complexation accounted for HREE enrichment as well in CPT and GW samples. Results of this study demonstrated significant potential for REE+Y recovery from AMD.

Acknowledgments

This investigation has been funded by National Natural Science Foundation of China (No. 41902243), Natural Science Foundation of Jiangxi province, China (20202BABL211018), and East China University of Technology Research Foundation for Advanced Talents (Nos. DHBK2019094 and SHT201901). We gratefully

612 acknowledge Dr. Michael Kersten for editing the manuscript in English and
613 comments. Dr Wei Xiu is thanked for his suggestions and comments. Anonymous
614 reviewers and Associate Editor Mae Sexauer Gustin are also acknowledged for their
615 helpful comments.

616

References

Akcil, A., Koldas, S. 2006. Acid Mine Drainage (AMD): causes, treatment and case studies. J. Clean. Prod. 14 (12- 13), 1139-1145.

Alonso, E., Sherman, A. M., Wallington, T. J., Everson, M. P., Field, F. R., Roth, R., Kirchain, R. E. 2012. Evaluating rare earth element availability: a case with revolutionary demand from clean technologies. Environ. Sci. Technol. 46(6), 3406-3414

Åström, M., Corin, N. 2003. Distribution of rare earth elements in anionic, cationic and particulate fractions in boreal humus-rich streams affected by acid sulphate soils. Wat. Res. 37, 273-280.

Åström, M. 2001. Abundance and fractionation patterns of rare earth elements in streams affected by acid sulphate soils. Chem. Geol. 175, 249-258.

Ayora, C., Macias, F., Torres, E., Lozano, A., Carrero, S., Nieto, J. M., Perez-Lopez, R., Fernandez-Martinez, A., Castillo-Michel, H., 2016. Recovery of rare earth elements and yttrium from passive-remediation systems of acid mine drainage. Environ. Sci. Technol. 50, 8255-8262.

Bau, M. 1999. Scavenging of dissolved yttrium and rare earths by precipitating iron oxyhydroxide: Experimental evidence for Ce oxidation, Y-Ho fractionation, and lanthanide tetrad effect. Geochim. Cosmochim. Acta 63, 67-77.

Binnemans, K., Jones, P. T., Blanpain, B., Van Gerven, T., Yang, Y., Walton, A., Buchert, M. 2013. Recycling of rare earths: a critical review. J. Clean. Prod. 51, 1-22.

639 Bozau, E., Leblanc, M., Seidel, J. L., Strk, H. J. 2004. Light rare earth elements
640 enrichment in an acidic mine lake (Lusatia, Germany). Appl. Geochem. 19(3),
641 261-271.
642 Cánovas, C. R., Macías, F., Olías, M., Basallote, M. D, Pérez-López, R, Ayora, C,
643 Nieto, J. M. 2020. Release of technology critical metals during sulfide oxidation
644 processes: the case of the Poderosa sulfide mine (south-west Spain). Environ.
645 Chem. 17, 93-104.
646 Chi, R. A., Liu, X. M. 2019. Prospect and development of weathered crust
647 elution-deposited rare earth ore. J. Chinese Rare Earth Soc. 37(2), 129-140.
648 De Carlo, E. H.; Wen, X. Y.; Irving, M. 1998. The influence of redox reactions on the
649 uptake of dissolved Ce by suspended Fe and Mn oxide particles. Aquat.
650 Geochem. 3, 357-389.
651 Dia, A., Gruau G., Olivié-Lauquet G., Riou C., Molénat J. and Curmi P. 2000. The
652 distribution of rare earth elements in groundwaters: Assessing the role of
653 source-rock composition, redox changes and colloidal particles. Geochim.
654 Cosmochim. Acta 64, 4131-4151.
655 Elderfield, J., Upstill-Goddard, R., Sholkovitz, E. R. 1990. The rare earth elements in
656 rivers, estuaries and coastal seas and their significance to the composition of
657 ocean waters. Geochim. Cosmochim. Acta 54, 971-991.
658 Gammons, C. H., Wood, S. A., Jonas, J. P., Madison, J. P. 2003. Geochemistry of rare
659 earth elements and uranium in the acidic Berkeley Pit Lake, Butte, Montana.
660 Chem. Geol. 198, 269-288.

661 Gimeno, M. J., Auqué, L. F., Nordstrom, D. K. 2000. REE speciation in
662 low-temperature acidic waters and the competitive effects of aluminium. Chem.
663 Geol. 165, 167-180.
664 Guo, H. M., Zhang, B., Wang, G. C., Shen, Z. L. 2010. Geochemical controls on
665 arsenic and rare earth elements approximately along a groundwater flow path in
666 the shallow aquifer of the Hetao Basin, Inner Mongolia. Chem. Geol. 270,
667 117-125.
668 Hao, X. Z., Wang, D. J., Wang, P. R., Wang, Y. X., Zhou D. M. 2016. Evaluation of
669 water quality in surface water and shallow groundwater: a case study of a rare
670 earth mining area in southern Jiangxi Province, China. Environ. Monit. Assess.
671 188(1), 24.
672 Haxel, G. B., Hedrick, J. B., Orris, G. J. 2002. Rare earth elements critical resources
673 for high technology. U.S. Geological Survey, Fact Sheet 087-02.
674 Hummel, W., Berner, U., Curti, E., Pearson, F. J., Thoenen, T. 2002. Nagra/PSI
675 Chemical Thermodynamic Data Base 01/01. Radiochim. Acta, 90, 805-813.
676 Janssen, R. P. T., Verweij, W., 2003. Geochemistry of some rare earth elements in
677 groundwater, Vierlingsbeek, The Netherlands. Water Res. 37, 1320-1350.
678 Johnson, D. B., Hallberg, K. B. 2005. Acid mine drainage remediation options: a
679 review. Sci. Total Environ. 338 (1), 3-14.
680 Léon, R., Macías, F., Cánovas, C. R., Pérez-López, R., Ayora, C., Nieto, J. M., Olías,
681 M. 2021. Mine waters as a secondary source of rare earth elements worldwide:
682 the case of the Iberian Pyrite Belt. J. Geochem. Explor. 224, 106742.

683 Leybourne, L., Goodfellow, W. D., Boyle, D. R., Hall, G. M. 2000. Rapid
684 development of negative Ce anomalies in surface waters and contrasting ree
685 patterns in groundwaters associated with Zn-Pb massive sulphide deposits. Appl.
686 Geochem. 15(6), 695-723.
687 Liu, Y., Zhong, X., Huot, H., Liu, W. S, Liu, C., Guo, M. N, Li, Y. Y, Fei, Y. H, Chao,
688 Y. Q, Wang, S. Z, Tang, Y. T., Qiu, R. L. 2020. Reclamation with organic
689 amendments and plants remodels the diversity and structure of bacterial
690 community in ion–adsorption rare earth element mine tailings. J. Soils Sediments
691 20, 3669-3680.
692 Liu, W. S., Wu, L. L., Zheng, M. Y., Chao, Y. Q., Zhao, C. M., Zhong, X., Ding, K. B.,
693 Huot, H., Zhang, M. Y., Tang, Y. T., Li, C., Qiu, R. L. 2019a. Controls on
694 rare-earth element transport in a river impacted by ion-adsorption rare-earth
695 mining. Sci. Total Environ. 660, 697-704.
696 Liu, W. S., Guo, M. N., Liu, C., Yuan, M., Chen, X. T., Huot, H., Zhao, C. M., Tang, Y.
697 T., Morel, J. L. Qiu, R. L. 2019b. Water, sediment and agricultural soil
698 contamination from an ion-adsorption rare earth mining area. Chemosphere, 216,
699 75-83.
700 Liu, H. Y., Guo, H. M., Wu, L. H. 2017a. Rare earth elements as indicators of
701 groundwater mixing in the North China Plain: A case study in the area of
702 Hengshui city, China. Pro. Earth Plant. Sci. 17, 396-399.
703 Liu, H. Y., Pourret, O., Guo, H. M., Bonhoure, J. 2017b. Rare earth elements sorption
704 to iron oxyhydroxide: Model development and application to groundwater. Appl.

Geochem. 87, 158-166.

Liu, H. Y., Guo, H. M., Xing, L. N., Zhan, Y. H., Li, F. L., Shao, J. L., Niu, H., Liang, X., Li, C. C. 2016. Geochemical behaviors of rare earth elements in groundwater along a flow path in the North China Plain. J. Asian Earth Sci. 117, 33-51.

Lozano, A., Ayora, C., Macías, F., Léon, R., Gimeno, M. J., Auqué, L. 2020a. Geochemical behavior of rare earth elements in acid drainages: modeling achievements and limitations. J. Geochem. Explor. 216, 106577.

Lozano, A., Ayora, C., Fernández-Martínez, A. 2020b. Sorption of rare earth elements on schwertmannite and their mobility in acid mine drainage treatments. Appl. Geochem. 113, 104499.

Luo, J. M., Huo, Y. W., Shen, Y. J., Hu, J. W., Ji, H. B. 2016. Effects of colloidal particle size on the geochemical characteristics of REE in the water in southern Jiangxi province, China. Environ. Earth Sci. 75, 81.

Luo, Y. R., Byrne, R. H. 2004. Carbonate complexation of yttrium and the rare earth elements in natural waters. Geochim. Cosmochim. Acta 68, 691-699.

Marquez, J., Pourret, O., Faucon, M. P., Weber, S., Hoàng, T., Martinez, R. 2018. Effect of cadmium, copper and lead on the growth of rice in the coal mining region of Quang Ninh, Cam-Pha (Vietnam). Sustainability, 10, 1758

Medas, D., Cidu, R., Giudici, G. D., Podda, F. 2013. Geochemistry of rare earth elements in water and solid materials at abandoned mines in SW Sardinia (Italy). J. Geochem. Explor. 133, 149-159.

Migaszewski, Z. M., Gałuszka, A., Gowska, S. 2016. Rare earth and trace element

727 signatures for assessing an impact of rock mining and processing on the
728 environment: Wiśniówka case study, south-central Poland. Environ. Sci. Pollut.
729 Res. 23, 24943-24959.
730 Migaszewski, Z., Gałuszka, A., Migaszewski, A. 2014. The study of rare earth
731 elements in farmer's well waters of the Podwiśniówka acid mine drainage area
732 (south-central Poland). Environ. Monit. Assessm. 186, 1609-1622.
733 Moraes, M. L., Ladeira, A. C. 2021. The role of iron in the rare earth elements and
734 uranium scavenging by Fe-Al precipitates in acid mine drainage. Chemosphere,
735 277, 130131.
736 Möller, P., Dulski, P., Gerstenberger, H., Morteani, G., Fuganti, A. 1998. Rare earth
737 elements, yttrium and H, O, C, Sr, Nd and Pb isotope studies in mineral waters
738 and corresponding rocks from NW-Bohemia, Czech Republic. Appl. Geochem.
739 13 (8), 975-994.
740 Nesbitt, H. W. 1979. Mobility and fractionation of rare earth elements
741 during weathering of a granodiorite. Nature, 279(19), 206.
742 Nordstrom, D. K., Blowes, D. W., Ptacek, C. J. 2015. Hydrogeochemistry and
743 microbiology of mine drainage: an update. Appl. Geochem. 57, 3-16.
744 Nordstrom, D. K., Alpers, C. N. The geochemistry of acid mine waters. In The
745 Environmental Geochemistry of Mineral Deposits: Chapter 6: Processes,
746 Methods and Health Issues; Plumlee, G.S., Logsdon, M.J., Eds.; Society of
747 Economic Geologists: Littleton, CO, USA, 1999; pp. 133-160.
748 Nozaki, Y., Zhang, J., Amakawa, H. 1997. The fractionation between Y and Ho in the

749 marine environment. Earth Planet. Sci. Lett. 148, 329-340.
750 Ogawa, Y., Ishiyama, D., Shikazono, N., Iwane, K., Hoshino, T., Kajiwara, M.,
751 Tsuchiya, N., Saini-Eidukat, B. Wood, S. A. 2019. Fractionation of rare earth
752 elements (REEs) and actinides (U and Th) originating from acid thermal water
753 during artificial and natural neutralization processes of surface waters. Geochim.
754 Cosmochim. Acta 249, 247-262.
755 Ohta, A., Kawabe, I. 2001. REE(III) adsorption onto Mn dioxide and Fe
756 oxyhydroxide: Ce(III) oxidation by Mn dioxide. Geochim. Cosmochim. Acta 65,
757 695-703.
758 Olías, M., Cánovas, C. R., Basallote, D. B., Lozano, A. 2018. Geochemical behaviour
759 of rare earth elements (REE) along a river reach receiving inputs of acid mine
760 drainage. Chem. Geol. 493, 468-477.
761 Parkhurst, D.L., Appelo, C.A.J. 2013. Description of input and examples for
762 PHREEQC version 3-a computer program for speciation, batch-reaction,
763 one-dimensional transport, and inverse geochemical calculations. US geological
764 survey techniques and methods, 6, 497.
765 Pérez-López, R., Delgado, J., Nieto J. M., Márquez-García, B. 2010. Rare earth
766 element geochemistry of sulphide weathering in the São Domingos mine area
767 (Iberian Pyrite Belt): a proxy for fluid-rock interaction and ancient mining
768 pollution. Chem. Geol. 276: 29-4.
769 Pourret, O., Houben, D. 2018. Characterization of metal binding sites onto biochar
770 using rare earth elements as a fingerprint. Heliyon, 4, e00543.

771 Pourret, O., Davranche, M. 2013. Rare earth element sorption onto hydrous
772 manganese oxide: A modeling study. J. Colloid interface Sci. 395, 18-23.
773 Pourret O., Davranche D., Gruau G., Dia A. 2007. Rare earth elements complexation
774 with humic acid. Chem. Geol. 243, 128-141.
775 Rodushkin, I., Paulukat, C., Pontér, S., Engström, E., Baxter, D. C., Sörlin, D.,
776 Pallavicini, N., Rodushkina, K. 2018. Application of double-focusing sector field
777 icp-ms for determination of ultratrace constituents in samples characterized by
778 complex composition of the matrix. Sci. Total Environ. 622-623, 203-213.
779 Schijf, J. Byrne R. H. 2004. Determination of $SO_4\beta_1$ for yttrium and the rare earth
780 elements at I = 0.66 m and T = 25 °C - Implications for YREE solution
781 speciation in sulfate-rich waters. Geochim. Cosmochim. Acta 68, 2825-2837.
782 Sharifi, R., Moore, F., Keshavarzi, B. 2013. Geochemical behavior and speciation
783 modeling of rare earth elements in acid drainages at sarcheshmeh porphyry
784 copper deposit, Kerman province, Iran. Chem. Erde - Geochem. 73(4), 509-517.
785 Smedley, P. L. 1991. The geochemistry of rare earth elements in groundwater from the
786 Carnmenellis area, southwest England. Geochim. Cosmochim. Acta 55,
787 2767-2779.
788 SMM. 2020. Shangai Metals Market. https://www.metal.com/ (accessed April 2021).
789 Stewart, B. W., Capo, R. C., Hedin, B. C., Hedin, R. S. 2017. Rare earth element
790 resources in coal mine drainage and treatment precipitates in the Appalachian
791 Basin, USA. Int. J. Coal Geol. 169, 28-39.
792 Sun, H. F., Zhao, F. H., Zhang, M., Z., Li, J. Q. 2012. Behavior of rare earth elements

in acid coal mine drainage in Shanxi province, China. Environ. Earth Sci. 67(1), 205-213.

Takahashi, Y., Manceau, A., Geoffroy, N., Marcus, M. A., Usui, A. 2007. Chemical and structural control of the partitioning of Co, Ce, and Pb in marine ferromanganese oxides. Geochim. Cosmochim. Acta 71(4), 984-1008.

Taylor, S. R. McClennan, S. M. 1988. The significance of the rare earths in geochemistry and cosmochemistry. In Handbook on the Physcis and Chemistry of the Rare Earths (eds. K. A. Gschneidner Jr and L. Eyring), Vol. 11, pp. 465-479, Elsevier, Amsterdam.

Tweed, S. O., Weaver, T. R., Cartwright, I., Schaefer, B. 2006. Behavior of rare earth elements in groundwater during flow and mixing in fractured rock aquifers: An example from the Dandenong Ranges, southeast Australia. Chem. Geol. 234, 291-307.

U.S. Geological Survey. Rare Earth Statistics, in Kelly, T.D., and Matos, G.R., comps., Historical Statistics for Mineral and Material Commodities in the United States: U.S. Geological Survey Data Series 140; US Geological Survey: Reston, Virginia, USA, 2014. Available online: http://minerals.usgs.gov/minerals/pubs/historicalstatistics/ (accessed on 14 August 2021).

Van Gosen, B. S., Verplanck, P. L., Long, K. R., Gambogi, J., Robert, R., Seal, I. I. The Rare-Earth Elements: Vital to Modern Technologies and Lifestyles (No. 2014-3078). Available online:

https://pubs.usgs.gov/fs/2014/3078/pdf/fs2014-3078.pdf (accessed on 5 April 2021).

Vass, C. R., Noble, A., Ziemkiewicz, P. F. 2019. The occurrence and concentration of rare earth elements in acid mine drainage and treatment by-products: part 1-initial survey of the northern Appalachian coal basin. Mining, Metall. Explor. 36(5), 903-916.

Vaziri Hassas, B., Rezaee, M., Pisupati, S.V. 2021. Effect of various ligands on the selective precipitation of critical and rare earth elements from acid mine drainage. Chemosphere 280, 130684

Verplanck, P. L., Nordstrom, D. K., Taylor, H. E., Kimball, B. A. 2004. Rare earth element partitioning between hydrous ferric oxides and acid mine water during iron oxidation. Appl. Geochem. 19, 1339-1354.

Wall, F. 2014. Rare earth elements. In: Gunn G. (Ed.) Critical Metals Handbook. John Wiley & Sons, Ltd., 312-339.

Wallrich, I. L., Stewart, B. W., Capo, R. C., Hedin, B. C., Phan, T. T. 2020. Neodymium isotopes track sources of rare earth elements in acidic mine waters. Geochim. Cosmochim. Acta 269, 465-483.

Wilkin, R. T., Lee, T. R., Ludwig, R. D., Wadler, C., Brandon, W., Mueller, B., Davis, E., Luce, D., Edwards, T. 2021. Rare-earth elements as natural tracers for in situ remediation of groundwater. Environ. Sci. Technol. 55 (2), 1251-1259.

Wood, S. A. 1993. The aqueous geochemistry of the rare-earth elements: critical stability constants for complexes with simple carboxylic acids at 25°C and 1 bar

and their application to nuclear waste management. Eng. Geol. 34, 229-259

Wood, S. A. 1990. The aqueous geochemistry of the rare-earth elements and yttrium: 2. Theoretical predictions of speciation in hydrothermal solutions to 350°C at saturation water vapor pressure. Chem. Geol. 88, 99-125

Worrall, F., Pearson, D. G. 2001. Water-rock interaction in an acidic mine discharge as indicated by rare earth element patterns. Geochim. Cosmochim. Acta 65(18), 3027-3040.

Yang, X. J., Li, A. J., Li, X. L., Wu, Y. D., Zhou, W. B., Chen, Z. H. 2013. China's ion-adsorption rare earth resources, mining consequences and preservation. Environ. Dev. 8 (1), 131-136.

Zhang, W., Honaker, R., 2020. Process development for the recovery of rare earth elements and critical metals from an acid mine leachate. Miner. Eng. 153, 106382

Zhang, J., Liu, C. Q. 2004. Major and rare earth elements in rainwaters from Japan and East China Sea: natural and anthropogenic sources. Chem. Geol. 209(3-4), 315-326.

Zhou, H. Y., Greig, A., Tang, J., You, C. F., Yuan D. X., Tong, X. N., Huang, Y. 2012. Rare earth element patterns in a Chinese stalagmite controlled by sources and scavenging from karst groundwater. Geochim. Cosmochim. Acta 83, 1-18.

Zhu, Z. Z., Liu, C. Q, Wang, Z. L., Liu, X. L., Li, J. 2016. Rare earth elements concentrations and speciation in rainwater from Guiyang, an acid rain impacted zone of southwest China. Chem. Geol. 442, 23-34.

860 **Figure captions**

861 **Figure 1** Study area and sampling locations (MW: mine water samples; NDT:
862 samples from nitrification-denitrification treatment process in a treatment plant;
863 CPT: samples from coagulating-precipitation treatment process in a treatment
864 plant: GW: groundwater sample; R: rock samples; SS: sediment samples; SG:
865 sludge samples)

866 **Figure 2** Piper plot of water sample compositions

867 **Figure 3** Changes of REE and Y with individual water samples ((a): pH, total REE
868 and Y (∑REE+Y), total Fe (Fe_T), Fe(II), Al and Mn concentrations; (b): SO_4^{2-}, Sr,
869 Rb, Zn, U, and Pb concentrations)

870 **Figure 4** Upper continental crust (UCC) normalized REE+Y patterns for water
871 samples and speciation modeling results ((a) and (b): MW sample; (c) and (d):
872 NDT sample; (e) and (f): CPT sample; (g) and (h): GW sample)

873 **Figure 5** Upper continental crust (UCC) normalized REE+Y patterns for rock,
874 sediment and sludge samples from mine water treatment (R: rock; SS: sediment:
875 SG: sludge)

876 **Figure 6** (a): a relationship between total REE+Y (∑REE+Y) and SO_4^{2-}, Al, Fe, and
877 Mn concentrations; (b): distinct fractionations of REE+Y; (c): Eh-pH diagram for
878 Ce-H_2O system (modified from Wilkin et al. (2021)); (d) a relationship between
879 pH and Ce/Ce*.

880

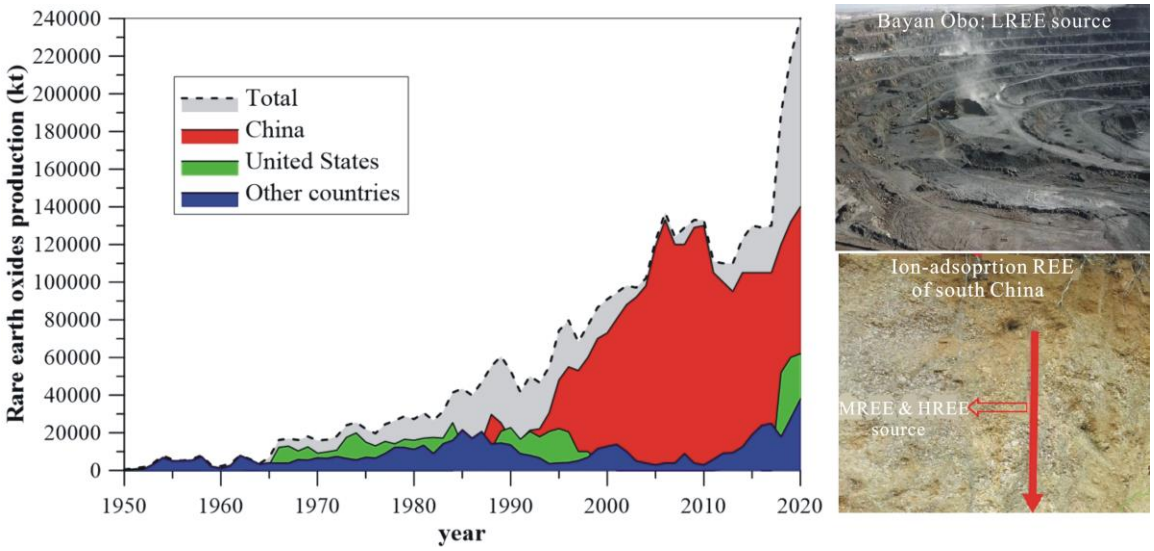

graphical abstract

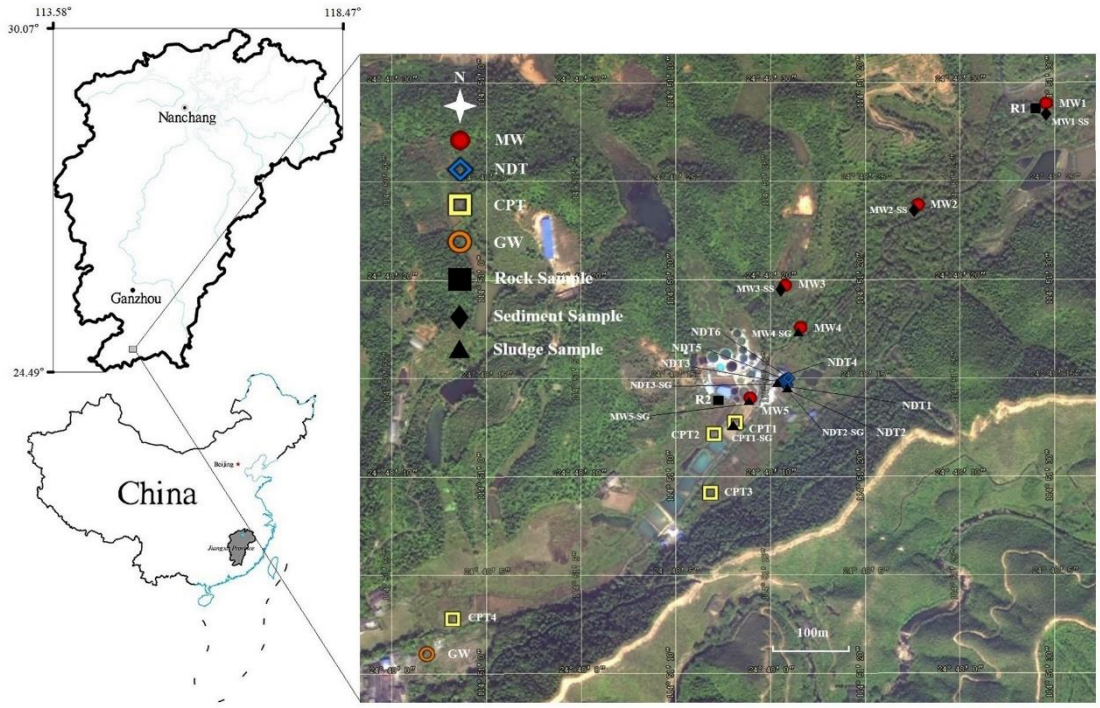
113.58°
118.47°
30.07°
24.49°
Nanchang
Ganzhou
China
N
MW
NDT
CPT
GW
Rock Sample
Sediment Sample
Sludge Sample
R1
MW1
MW1-SS
MW2-SS
MW2
MW3-SS
MW3
NDT6
MW4-SG
MW4
NDT5
NDT3
NDT4
NDT3-SG
R2
MW5
MW5-SG
NDT1
CPT2
CPT1
CPT1-SG
NDT2-SG
NDT2
CPT3
CPT4
GW
100m

Fig. 1

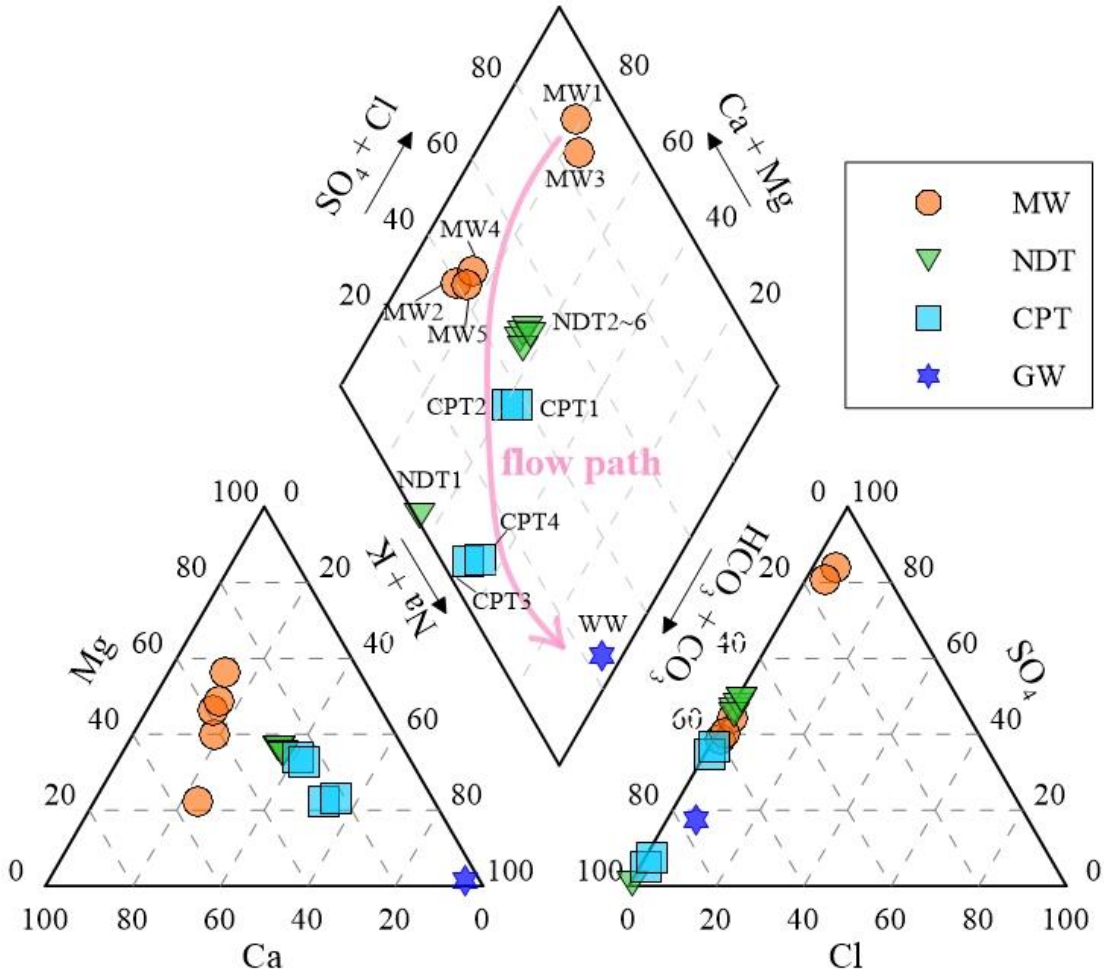
MW1
MW3
MW4
MW2
MW5
NDT2~6
CPT2
CPT1
NDT1
CPT4
CPT3
WW
flow path
MW
NDT
CPT
GW
SO4 + Cl
Ca + Mg
Na + K
HCO3 + CO3
Mg
Ca
Cl
SO4

Fig. 2

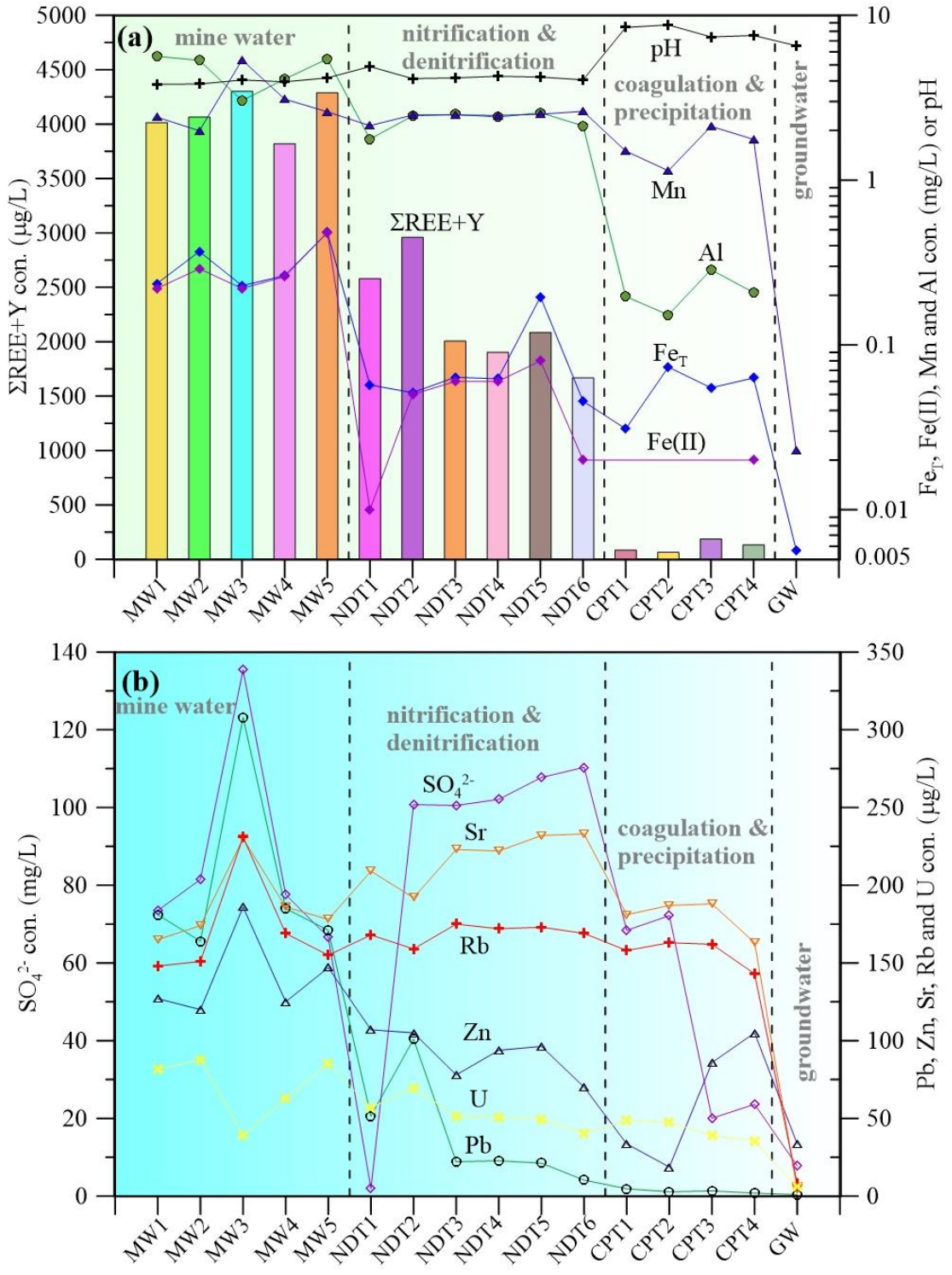
(a)
mine water
nitrification &
denitrification
coagulation &
precipitation
groundwater
pH
Mn
Al
ΣREE+Y
Fe$_T$
Fe(II)
ΣREE+Y con. (μg/L)
Fe$_T$, Fe(II), Mn and Al con. (mg/L) or pH
(b)
mine water
nitrification &
denitrification
coagulation &
precipitation
groundwater
SO$_4^{2-}$
Sr
Rb
Zn
U
Pb
SO$_4^{2-}$ con. (mg/L)
Pb, Zn, Sr, Rb and U con. (μg/L)
MW1
MW2
MW3
MW4
MW5
NDT1
NDT2
NDT3
NDT4
NDT5
NDT6
CPT1
CPT2
CPT3
CPT4
GW

Fig. 3

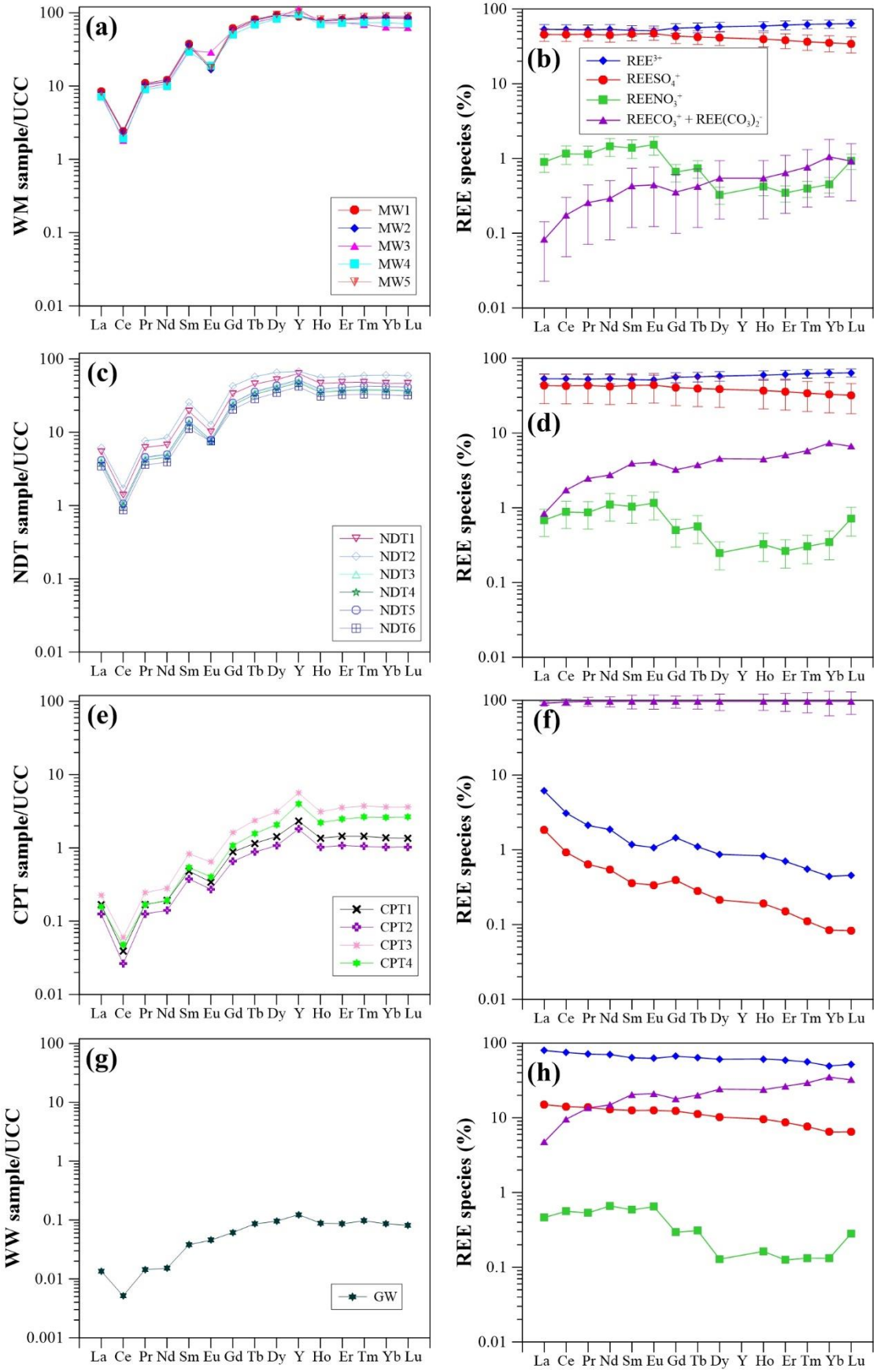
(a)
WM sample/UCC
MW1
MW2
MW3
MW4
MW5
(b)
REE species (%)
REE3+
REESO4+
REENO3+
REECO3+ + REE(CO3)2-
(c)
NDT sample/UCC
NDT1
NDT2
NDT3
NDT4
NDT5
NDT6
(d)
REE species (%)
(e)
CPT sample/UCC
CPT1
CPT2
CPT3
CPT4
(f)
REE species (%)
(g)
WW sample/UCC
GW
(h)
REE species (%)
La Ce Pr Nd Sm Eu Gd Tb Dy Y Ho Er Tm Yb Lu

907

908 Fig. 4

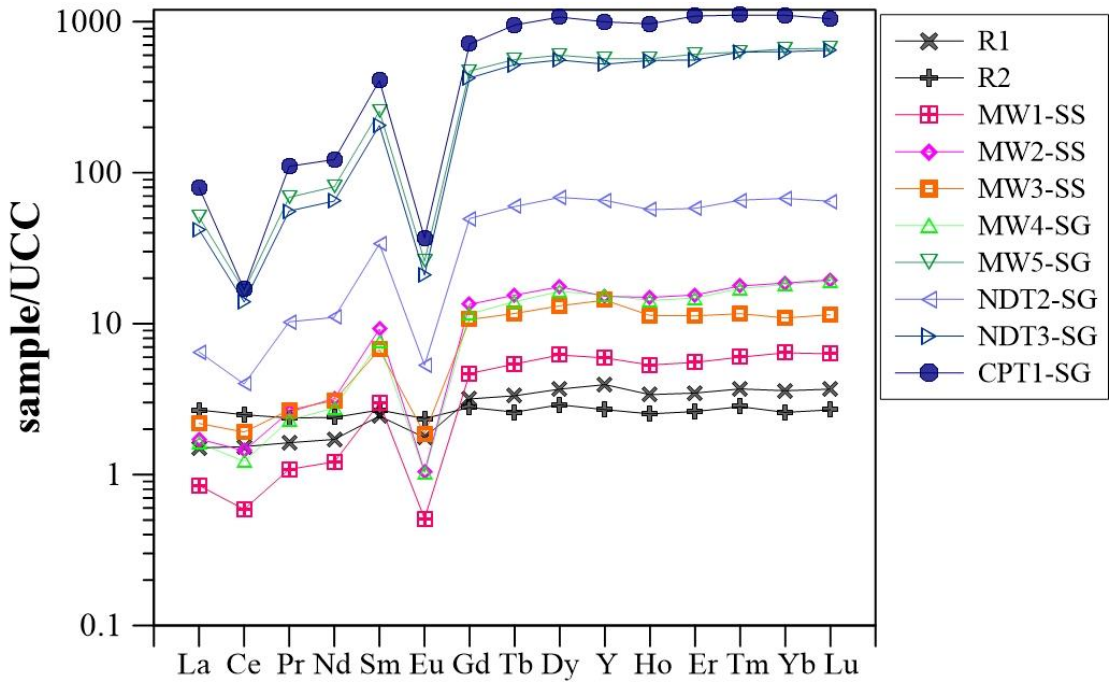

909

910 Fig. 5

911

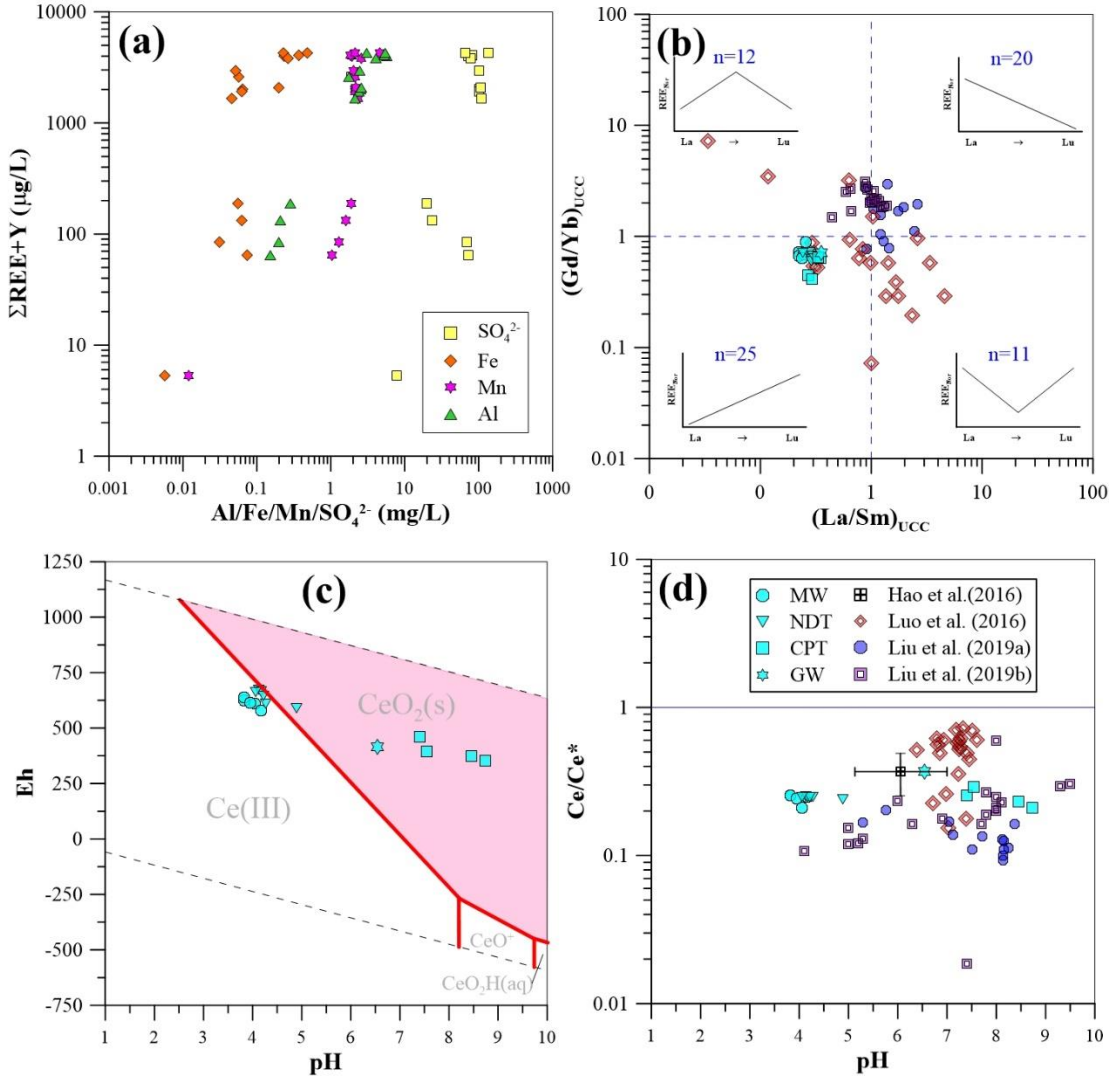

912

913 Fig. 6

914

915